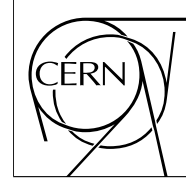


The Compact Muon Solenoid Experiment

CMS Note

Mailing address: CMS CERN, CH-1211 GENEVA 23, Switzerland



July 2002

Observing anomalous di-boson couplings in $Z\gamma\gamma$ and $ZZ\gamma$ vertices at CMS

C. K. Mackay

Department of Physics, University of Bristol, Bristol, UK.

P. R. Hobson

Department of Electronic and Computer Engineering, Brunel University, Uxbridge, UK.

Abstract

This note presents a study of the anomalous couplings, h_1^V , h_2^V , h_3^V and h_4^V ($V=Z,\gamma$), of the $Z\gamma\gamma$ and $ZZ\gamma$ vertices. An independent NLL Monte Carlo event generator has been combined with the CMSJET detector simulation to provide a realistic simulation of the process at CMS. The methods to determine the presence of anomalous couplings have been evaluated. We show that the photon transverse momentum spectrum and the transverse mass of the $(\ell\ell\gamma)$ are the most sensitive to Standard Model deviations and can be used to provide improved sensitivities of the anomalous couplings at the LHC energies.

1 Introduction

The previous studies of the $W\gamma$ vertex [1] [2] anomalous couplings at the LHC show that CMS will be able to obtain greatly improved sensitivities of the anomalous couplings in this vertex. This note presents a similar study for the $ZZ\gamma$ and $Z\gamma\gamma$ vertices. The signal from the $Z\gamma$ signal has been studied for both SM and anomalous couplings and methods to obtain limits on the couplings are discussed.

2 Anomalous Couplings Of Gauge Bosons

A direct measurement of vector boson couplings is possible via pair production processes like $q\bar{q} \rightarrow W^+W^-$, $W\gamma$, $Z\gamma$, WZ and by trilinear boson production such as WWW , $WW\gamma$, $ZZ\gamma$ and $Z\gamma\gamma$. A precise and direct measurement of the trilinear and quartic couplings of the electroweak vector bosons and the demonstration that they agree with the SM would beautifully corroborate spontaneously broken, non-Abelian gauge theories as the basic structure describing the fundamental interactions of nature [3].

The trilinear and quartic couplings probe different aspects of the weak interactions. The trilinear couplings test non-Abelian gauge structure where deviations from the SM can result from integrating out heavy particles in loops [4]. In contrast the quartic couplings can be regarded as a window for electroweak symmetry breaking. The quartic couplings represent a connection to the scalar sector of the theory.

However, a measure of the vertices may also be used to probe for new physics. It is possible in principle that signals for new physics beyond the SM will appear in this sector through *anomalous* trilinear (or quartic) gauge boson vertices. It is possible that the quartic couplings deviate from their SM values while the trilinear couplings do not. Gauge boson pair production in hadronic collisions provides an opportunity to probe the structure of triple gauge boson vertices in a direct and essentially model independent way. The triple gauge boson coupling is fixed by the $SU(2)$ symmetry of the SM.

In the SM, the three boson vertices come from the non-commutative part of the $SU(2)\oplus U(1)$ gauge symmetry. The gauge boson portion of the Lagrangian in the SM is given by Eqn. 1 [5]:

$$L_g = -\frac{1}{4}G_{\mu\nu}^j G^{j\mu\nu} - \frac{1}{4}B_{\mu\nu}B^{\mu\nu} \quad (1)$$

where $B_{\mu\nu} = \partial_\mu B_\nu - \partial_\nu B_\mu$, $G_{\mu\nu}^j = \partial_\mu W_\nu^j - \partial_\nu W_\mu^j + gf_{jkl}W_\mu^k W_\nu^l$, B is the electromagnetic field tensor, W is the weak field tensor g is the coupling constant and f_{jkl} are the structure constants of the weak isospin group.

Hadron colliders are able to produce gauge boson pairs in both charged and neutral final states, but only the W^+W^- , $W^\pm\gamma$, $Z\gamma$ and $W^\pm Z$ channels give a triple gauge boson vertex contribution. Studying the W^+W^- channel is very difficult. If the W 's decay hadronically the large QCD background is two orders of magnitude higher in cross-section[6] [7], if the W 's decay leptonically the $t\bar{t}\gamma$ background increases the difficulty of observing the signal [8]. It is also sensitive to both the $WW\gamma$ and WWZ couplings via the s-channel [9]. In contrast, the $W^\pm\gamma$ and $W^\pm Z$ channels are particularly interesting since their backgrounds can be suppressed and they are easy to isolate compared with the W^+W^- pair production [3] [9]. The sensitivities of CMS to the $WW\gamma$ vertex at LHC energies has been studied [1] [10] [11]. This study investigates the possibility of observing anomalous couplings of the $ZZ\gamma$ vertex and the $Z\gamma\gamma$ vertex at the LHC using the CMS detector.

If anomalous couplings exist, they must be parameterised so that experimentalists can study them. In the absence of a specific model of new physics, effective Lagrangian techniques are extremely useful. An effective Lagrangian [12] parameterises, in a model independent way, the low energy effects of the new physics to be found at high energies. It is necessary only to specify the particle content and the symmetries of the low-energy theory. Although effective Lagrangians contain an infinite number of terms, they are organised in powers of $1/\Lambda$ where Λ is the scale of new physics [13] [14]. Thus at energies which are low compared to Λ only the first few terms of the effective Lagrangian are important.

2.1 The $ZV\gamma$ Vertex

In $q\bar{q} \rightarrow Z\gamma$, both the time-like virtual photon and/or Z boson couple to essentially massless fermions, which ensures that effectively $\partial_\mu V^\mu=0$, $V=Z,\gamma$. This condition, together with Lorentz invariance of the on-shell photon and electromagnetic gauge invariance restricts the tensor structure of the $ZV\gamma$ vertex to allow only four free parameters. Eqn. 2 shows the most general nonstandard $ZZ\gamma$ vertex function [15]:

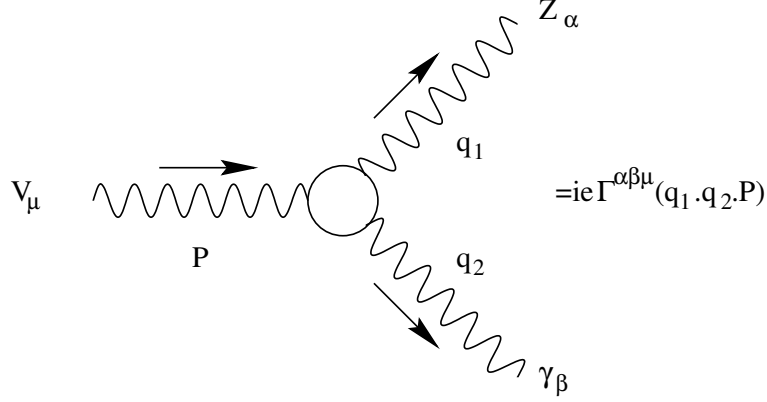


Figure 1: Feynman rule for the general $Z\gamma V$, $V=Z,\gamma$ vertex. The vertex function Γ is given in Eqn. 2. e is the charge of the proton

$$\Gamma_{Z\gamma Z}^{\alpha\beta\mu}(q_1, q_2, P) = \frac{P^2 - q_1^2}{m_Z^2} \left[h_1^Z (q_2^\mu g^{\alpha\beta} - q_2^\alpha g^{\mu\beta}) + \frac{h_2^Z}{m_Z^2} P^\alpha [(P \cdot q_2) g^{\mu\beta} - q_2^\mu P^\beta] + h_3^Z \epsilon^{\mu\alpha\beta\rho} q_{2\rho} + \frac{h_4^Z}{m_Z^2} P^\alpha \epsilon^{\mu\beta\rho\sigma} P_\rho q_{2\sigma} \right] \quad (2)$$

where m_Z is the Z-boson mass and the notation is given in Fig. 1.

The form factors h_i^V are dimensionless functions of q_1^2 , q_2^2 and P^2 . All couplings are C odd; h_1^V and h_2^V violate CP while h_3^V and h_4^V conserve CP. Combinations of h_3^V (h_1^V) and h_4^V (h_2^V) correspond to the electric (magnetic) dipole and magnetic (electric) quadrupole transition moment. Within the standard model, at tree level, all couplings h_i^V vanish.

To avoid violating unitarity form factors are introduced to limit the scattering amplitude at high energies. The form factors are chosen such that [16]:

$$h_i^V(m_Z^2, 0, \hat{s}) = \frac{h_{i0}^V}{(1 + \hat{s}/\Lambda^2)^n} \quad (3)$$

Both the unitarity limits and the strength of the couplings depend strongly on the scale parameter Λ . Together with the denominator power n , Λ is a parameter of the model. As long as the choice of n is fixed, the scale Λ is the only free parameter. The exponent $n=3$ ($n=4$) is chosen for h_3^V (h_4^V) in order to suppress $ZV\gamma$ production at energies $\sqrt{\hat{s}} \gg \Lambda \gg M_Z$ [17], where novel phenomena such as resonance or multiple weak boson production are expected to be important. The actual scale of Λ is not predicted by the theory. The physical meaning of this parameter is a ‘‘compositeness scale’’, or a scale for new physical phenomena. If Λ is too small ($\sim M_Z$), one would expect the real W and Z bosons to have properties different from what the SM predicts, but there has been no evidence of this experimentally. Very large values of Λ (~ 10 TeV) would suppress any effects of the anomalous couplings due to the unitarity limits up to high energies, which is unnatural. The value of Λ must be carefully chosen prior to setting the limits on anomalous couplings. This study investigates one value of Λ chosen to coincide with the scales currently used at the Tevatron and LEP: $\Lambda = 750$ GeV. Unitarity itself imposes limits on the anomalous $ZV\gamma$ couplings of [16]:

$$|h_{10}^{Z/\gamma}|, |h_{30}^{Z/\gamma}| < \frac{(\frac{2}{3}n)^n}{(\frac{2}{3}n-1)^{n-3/2}} \cdot \frac{0.126/0.151TeV^3}{\Lambda^3} \quad (4)$$

$$|h_{20}^{Z/\gamma}|, |h_{40}^{Z/\gamma}| < \frac{(\frac{2}{5}n)^n}{(\frac{2}{5}n-1)^{n-5/2}} \cdot \frac{2.1/2.5 \times 10^{-3}TeV^5}{\Lambda^5} \quad (5)$$

When these bounds are observed, tree level unitarity is satisfied throughout the entire \hat{s} range, provided one anomalous coupling is non-vanishing at a time. If more than one coupling contributes, the unitarity bounds differ slightly [16] [17].

The contribution of the $ZV\gamma$ diagram to the helicity amplitudes can be written as [16] [17]:

$$\Delta M^V(\sigma, \bar{\sigma}, \lambda_Z, \lambda_\gamma) = -\sqrt{2}e^2 g_{2\sigma}^{Vf\bar{f}} \frac{\hat{s}}{\hat{s} - m_V^2} \left(1 - \frac{m_Z^2}{\hat{s}}\right) \partial_\sigma, -\bar{\sigma} A_{\lambda_Z \lambda_\gamma}^V X d_{\sigma-\bar{\sigma}, \lambda_Z-\lambda_\gamma}^1(\Theta) \quad (6)$$

where $\sigma, \bar{\sigma}$ and $\lambda_Z, \lambda_\gamma$ denote the helicities of the particles involved and $g_{2\sigma}^{Vf\bar{f}}$ is the $Vf\bar{f}$ SM coupling constant. The dependence on the centre of mass scattering angle Θ is given by the conventional d functions [18].

2.2 Previous Studies of $ZV\gamma$ Interactions

So far there have been several experimental studies of the $ZV\gamma$ vertex. The vertex has been tested both indirectly, in low energy experiments, and directly at CERN(LEP) and at FERMILAB(CDF and D0). Some of the more recent results are presented here.

2.2.1 Low energy, indirect tests

Low energy experiments are sensitive to the anomalous couplings via loop corrections that arise in penguin type diagrams. However, unlike direct tests, these results are sensitive to the regularization schemes and loop cut off parameters used in the calculations. This sensitivity makes the results model dependent and somewhat controversial. A further difficulty is that the limits on anomalous couplings obtained from indirect tests have the shape of bands that stretch to infinity when both couplings are allowed to vary¹⁾. However, if one parameter is fixed, the limits on the second parameter can be very tight.

2.2.2 $e^+e^- \rightarrow W^+W^-$ at LEP

During its second phase of operation, from 1996 until November 2000, the LEP e^+e^- collider at CERN increased its centre-of-mass energy from 161 GeV up to 209 GeV in the final year. A total integrated luminosity of approximately 700 pb^{-1} per experiment was recorded. The channels used in the analysis are $e^+e^- \rightarrow q\bar{q}\gamma(\gamma)$ and $e^+e^- \rightarrow \nu\bar{\nu}\gamma(\gamma)$. The LEP [19] average 95% confidence level limits are shown in Table. 1.

2.2.3 $q\bar{q} \rightarrow Z\gamma$ at the Tevatron

Both CDF and D0 have observed $Z\gamma$ events in the electron, muon and neutrino decay modes of Z bosons produced at $\sqrt{s} = 1.8 \text{ TeV}$. The best results are from the D0 experiment where 89 fb^{-1} of data were collected. The combined results for all channels with a form factor scale of $\Lambda = 750 \text{ GeV}$ are[20]:

$$|h_3^Z| < 0.36 \quad (|h_4^Z| = 0); \quad |h_4^Z| < 0.05 \quad (|h_3^Z| = 0)$$

$$|h_3^\gamma| < 0.37 \quad (|h_4^\gamma| = 0); \quad |h_4^\gamma| < 0.05 \quad (|h_3^\gamma| = 0)$$

¹⁾ Direct tests from $ZZ\gamma$ and $Z\gamma\gamma$ production produce closed contour limits because the total production cross section for any pair of couplings is bilinear

Table 1: Combined limits from the LEP experiments

95 % CL Limits	
CP-violating	CP-conserving
$-0.15 < h_1^Z < 0.14$	$-0.22 < h_3^Z < 0.07$
$-0.10 < h_2^Z < 0.10$	$-0.05 < h_4^Z < 0.15$
$-0.09 < h_1^\gamma < 0.05$	$-0.07 < h_3^\gamma < -0.002$
$-0.05 < h_2^\gamma < 0.05$	$0.002 < h_4^\gamma < 0.05$

2.2.4 Predicted Results From Forthcoming Experiments

Before the LHC turns on the Tevatron will have had several years more data taking following its upgrade. Initial studies suggest the Tevatron will be able to decrease the limits by nearly two orders of magnitude [21]. Table 2 shows the predicted limits on the anomalous couplings for $ZZ\gamma$ production from 1 and 10 fb^{-1} of data at the Tevatron's next run.

Table 2: Predicted limits from run 2 at the Tevatron

Luminosity	h_3^Z	h_4^Z
1 fb^{-1}	$-0.18 < h_3^Z < 0.18$	$-0.0115 < h_4^Z < 0.0115$
10 fb^{-1}	$-0.09 < h_3^Z < 0.09$	$-0.005 < h_4^Z < 0.005$

The qualitative differences between the results at the Tevatron and the LHC will be due to the differences between $p\bar{p}$ and pp scattering and the ranges of x probed. At the Tevatron, $Z\gamma$ production in $p\bar{p}$ collisions is dominated by valence quark interactions. The valence quark distributions increase with Q^2 for the x values probed at the Tevatron. At the LHC, sea quark interactions dominate in the pp process and smaller x values are probed. The sea quark distributions increase with Q^2 for the x values probed at the LHC. Thus the Born cross section decreases slightly with Q^2 at the Tevatron but increases with Q^2 at the LHC.

3 Simulation of the process $pp \rightarrow Z\gamma + \text{jet}$

In order to set limits in the $ZV\gamma$ anomalous couplings at CMS we must be able to simulate the process and the response of the detector. The event generator should take into account the interference effects between production, trilinear and decay diagrams and be capable of calculating total and differential cross sections of the reaction for both SM and anomalous cases. The overall Monte Carlo must also simulate the response of the various parts of the CMS detector, taking into account particle identification efficiencies, trigger efficiencies, etc. In addition, it must be capable of coping quickly with a large number of events. This is essential as the effects of anomalous couplings are only pronounced at high $p_T(\gamma)$, where the SM cross section is very small. A large number of generated events in the high photon transverse momentum region are required in order to make a precise fit to the $p_T(\gamma)$ spectrum. These must be generated for the SM and a range of values of the anomalous couplings.

3.1 $Z\gamma$ Event Generator

Currently there are two event generators which incorporate the $Z\gamma$ matrix elements. The first, PYTHIA, [22] is only capable of generating SM $Z\gamma$ events. It does not include higher order QCD corrections which are important at the LHC. Therefore it is not useful in this case and has not been investigated. The second generator, of U. Baur [17] (referred to here as BAUR), includes the full set of next-to-leading logarithmic (NLL) matrix elements necessary to calculate the process and also calculates the contributions of all the couplings. The BAUR generator also includes the NLL QCD corrections which will be very large at the LHC [23].

In this study only the next-to-leading logarithmic (NLL) generator has been studied. Previous studies have compared the leading order to the next-to-leading order [24] and as the NLL QCD corrections will be so important at

the LHC the LO has not been investigated here.

The input parameters for the generator were $M_t = 175$ GeV, $M_Z = 91.1$ GeV, $\sin^2\theta_W = 0.23$ and $\sqrt{\hat{s}} = 14$ TeV. The values of the theoretical soft and collinear cutoff parameters δ_s and δ_c used were $\delta_s = 0.08$ and $\delta_c = 0.05$. Appendix I explains the choice of values for these parameters. The parton distribution functions used were the updated leading order Duke-Owens set 1 (DO1.1) [25] with the Q^2 scale given by the centre-of-mass squared, \hat{s} . While this is an appropriate parton distribution function to use it would be interesting in future studies to examine the use of different functions.

The generator gave only the energy and x and z components of the particles' four-momenta. Therefore the whole event was rotated about the z axis by a randomly generated angle between 0 and 2π radians, to provide a y momentum component. The output from the event generator consists of the 4-momenta of the lepton and neutrino from the Z decay, the photon and the quark (for the 4-body process).

3.2 Generator and Detector Simulation

The output of the BAUR generator (4-momenta of the final state particles) was used as an input for an adapted version of CMSJET (see Appendix) to provide an event generator and detector simulation for the $Z\gamma$ process at the CMS detector. The 4-momenta of the photon and leptons can be put straight into CMSJET. However, as the jet is so far only a quark, this must first be put into Pythia, assigned a flavour and fragmented. The quark type is randomly assigned as u, \bar{u} , d or \bar{d} . No colour matching was used in this simulation. Following fragmentation of the quark the 4-vectors of all the jet constituents are put into CMSJET. The lepton and neutrino type can be determined by the user within CMSJET.

The BAUR generator outputs the four vectors of the $Z\gamma$ events into an Ntuple. This Ntuple is then the input for the adapted version of CMSJET 4.3 which then passes each event through the detector and any events passing the user defined cuts are put into a second Ntuple which is then analysed.

4 The $Z\gamma$ Signal

The Z boson is a massive particle and thus decays quickly to lighter particles. The Z boson can decay into a pair of leptons or into hadrons. The hadronic decay mode of the Z boson will be overwhelmed by the large QCD background at the LHC [26]. The only mode where a significant signal will be seen is the leptonic mode. One of the leptonic decay modes, $Z \rightarrow \tau\bar{\tau}$, is experimentally very challenging; thus only the electron and muon channels are considered. The branching fractions for these two decay modes as measured by the LEP experiments at CERN are [27]:

$$B = \text{Br}(Z \rightarrow e\bar{e}) = 3.367 \pm 0.005 \%$$

$$B = \text{Br}(Z \rightarrow \mu\bar{\mu}) = 3.367 \pm 0.008 \%$$

The leading order Feynman diagrams involving Z production that produce a final state of $\ell\bar{\ell}\gamma$ are shown in Fig. 2a-d. The first two diagrams (a and b) represent the initial state radiation where one of the incoming partons emits a hard photon by *bremssstrahlung*. Diagram (c) is the trilinear coupling ($ZV\gamma$ vertex) and is the only diagram that is affected by the anomalous couplings. Diagram (d) is the final state *bremssstrahlung* production.

There is also the Z decay into a pair of neutrinos, where the experimental signal is

$$p\bar{p} \rightarrow p_{T(miss)}\gamma$$

where the missing transverse momentum $p_{T(miss)}$ results from the non-observation of the neutrino pair.

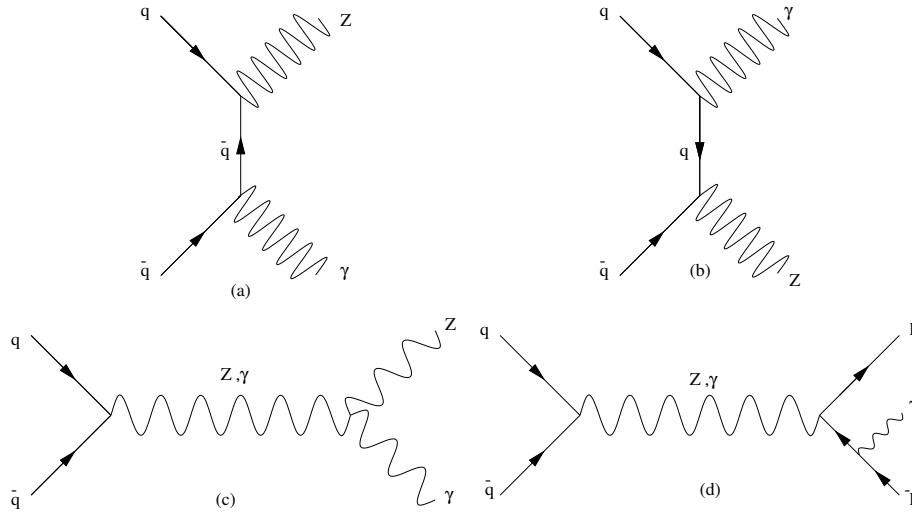


Figure 2: Leading order Feynman diagrams for the $q\bar{q} \rightarrow Z\gamma$ in the SM (a,b), anomalous couplings (c) and final-state radiation (d)

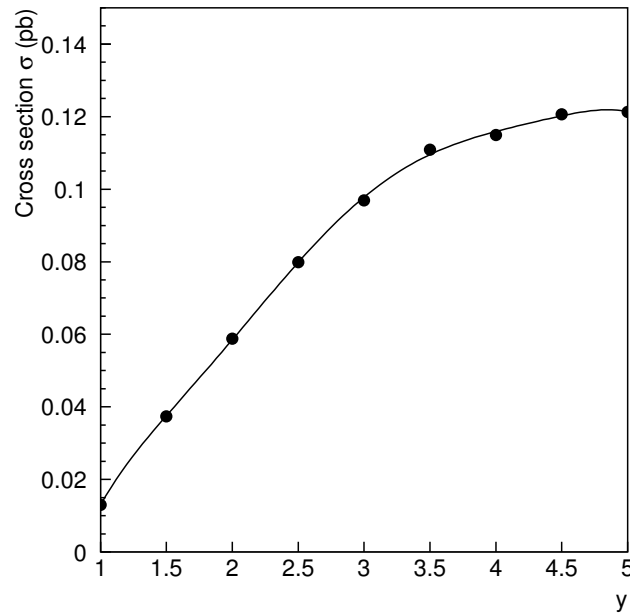


Figure 3: Cross section as a function of rapidity for SM values of $h_i^V (=0)$

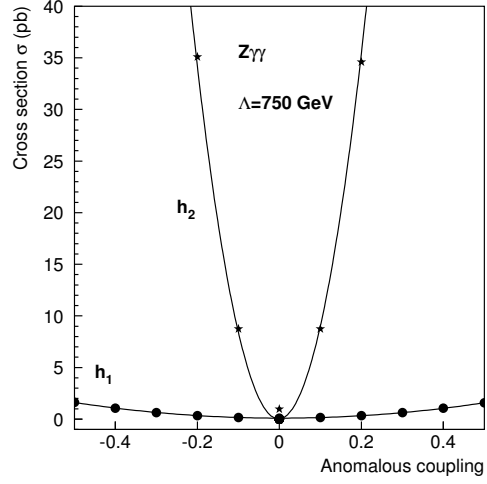
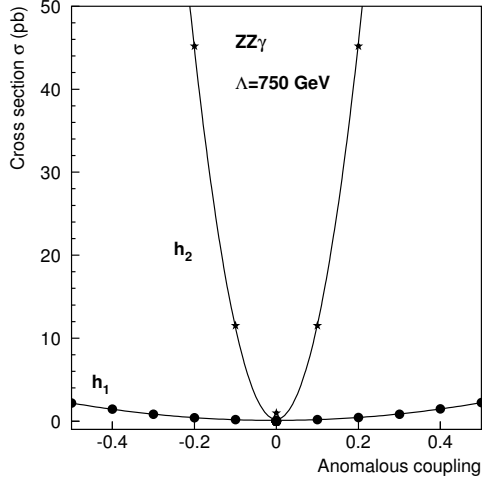


Figure 4: Cross section \times branching ratio as a function of the CP-violating anomalous couplings h_1^V and h_2^V for (left) $ZZ\gamma$ and (right) $Z\gamma\gamma$ production.

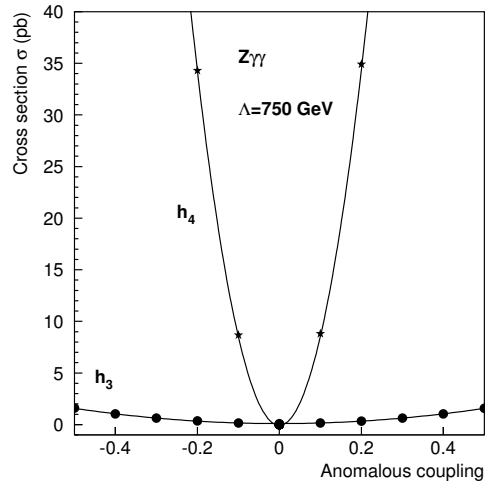
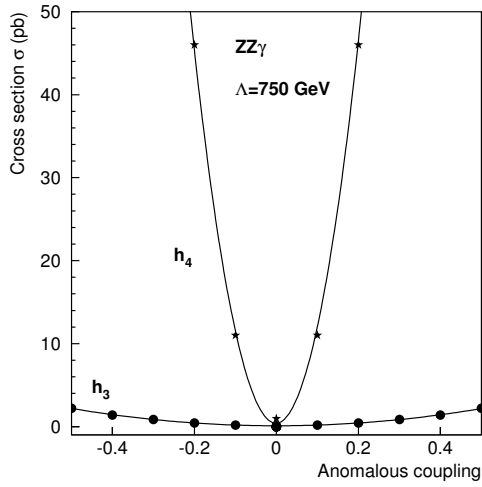


Figure 5: Cross section \times branching ratio as a function of the CP-conserving anomalous couplings h_3^V and h_4^V for (left) $ZZ\gamma$ and (right) $Z\gamma\gamma$ production.

The Monte Carlo generator for the SM and anomalous coupling processes that are shown in Fig. 2 were provided by the theoretical calculations of U. Baur [17]. The generator takes into account the finite Z-width effects and interference effects and next to leading order (NLO) effects. All the calculations are done for the LHC energy ($\sqrt{s} = 14$ TeV).

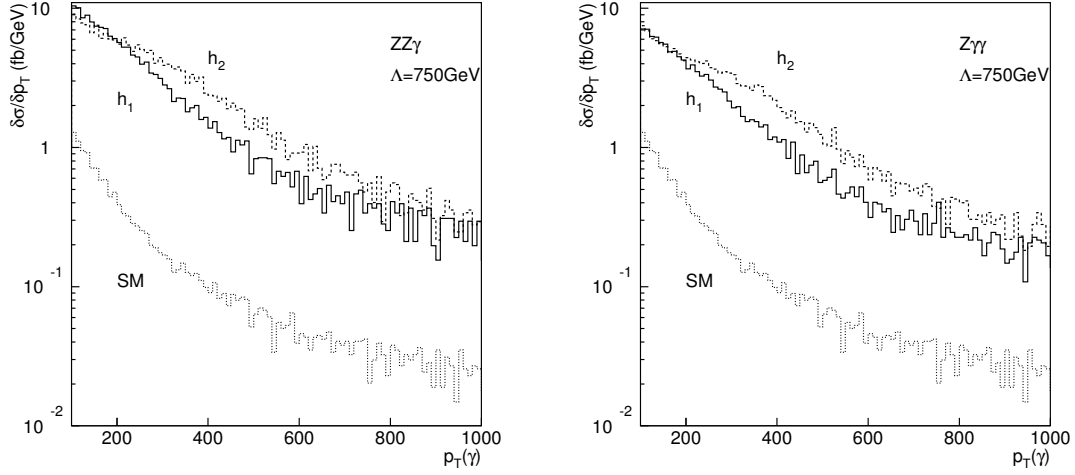


Figure 6: $d\sigma/dp_T(\gamma)$ spectrum for the SM ($h_i^V=0$) and anomalous CP-violating coupling limits ($h_1^V=0.5$ and $h_2^V=0.05$) at $\Lambda = 750$ GeV for (left) the $ZZ\gamma$ vertex and (right) the $Z\gamma\gamma$ vertex

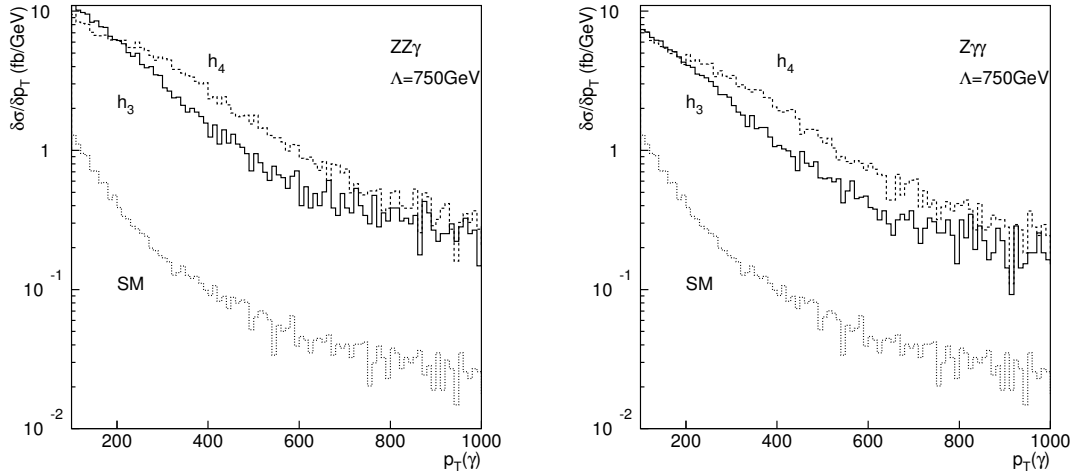


Figure 7: $d\sigma/dp_T(\gamma)$ spectrum for the SM ($h_i^V=0$) and anomalous CP-conserving coupling limits ($h_3^V=0.5$ and $h_4^V=0.05$) at $\Lambda = 750$ GeV for (left) the $ZZ\gamma$ vertex and (right) the $Z\gamma\gamma$ vertex

The cross section varies as a function of rapidity. Fig. 3 shows the cross section \times branching ratio as a function of rapidity for the SM values of the couplings $h_i^V (=0)$. This study makes cuts of the p_T of the individual particles: $p_T(\gamma) > 70$ GeV, $p_T(\ell^\pm) > 15$ GeV and $p_T(\text{jet}) > 10$ GeV. Cuts are also made on $\Delta R_{\ell\gamma} > 0.7$ and on the invariant mass of the charged lepton pair, $M_{\ell\ell} > 10$ GeV. Without finite $M_{\ell\ell}$, $p_T(\gamma)$, $p_T(\ell^\pm)$ cuts, the cross section for $p\bar{p} \rightarrow \ell^+\ell^-\gamma$ would diverge.

Any anomalies in the $ZZ\gamma$ and $Z\gamma\gamma$ couplings will manifest themselves as an excess of events over the SM prediction, due to the contribution of the s-channel diagram. Fig. 4 shows the cross section \times branching ratio for $pp \rightarrow Z(\ell^+, \ell^-)\gamma$ as a function of the two CP-violating coupling parameters, h_1^V and h_2^V . Fig. 5 shows the cross section \times branching ratio for $pp \rightarrow Z(\ell^+, \ell^-)\gamma$ as a function of the two CP-conserving coupling parameters, h_3^V and h_4^V . Away from the SM values of $h_i^V = 0$ an excess of events is observed. The cross section has a minimum at the SM values and can be expressed as a bilinear form of the anomalous couplings. By comparing the measured total cross-section to the theoretical predictions, limits can be set on the anomalous couplings.

There is a variation in cross section between $ZZ\gamma$ and $Z\gamma\gamma$ production with anomalous coupling. The $ZZ\gamma$ production provides approximately a factor 2 more cross section for all the couplings than the $Z\gamma\gamma$ production. It is also clear from Figs. 4 and 5 that the anomalous couplings h_2^V and h_4^V produce a much greater increase in cross section than the couplings h_1^V and h_3^V .

The $ZZ\gamma$ vertex yields enhancements in the $Z\gamma$ cross section, especially at large values of the photon transverse momentum ($p_T(\gamma)$). If non-standard couplings exist, the cross section for high p_T photons increases drastically. The $p_T(\gamma)$ distribution is the most sensitive indicator of anomalous couplings since it is a directly observable quantity. The change in shape of the p_T distribution is due to a combination of the destructive interference in the $Z\gamma$ Born subprocess and a logarithmic enhancement factor in the $q\bar{q}$ and $\bar{q}g$ real emission subprocesses.

Fig. 6 shows the $d\sigma/dp_T(\gamma)$ spectrum for different CP-violating anomalous coupling constants: the SM ($h_i^V=0$), the tightest current limit on $h_1^V (=0.5$ with $h_2^V=0$), and the tightest current limit on $h_2^V (=0.05$ with $h_1^V=0$). Fig. 7 shows the $d\sigma/dp_T(\gamma)$ spectrum for different CP-conserving anomalous coupling constants: the SM ($h_i^V=0$), the tightest current limit on $h_3^V (=0.5$ with $h_4^V=0$), and the tightest current limit on $h_4^V (=0.05$ with $h_3^V=0$). A form factor scale of $\Lambda=750$ GeV was used. The variation in the distribution due to the anomalous couplings is clearly visible. The cuts used in Figs. 6 and 7 were $\eta < \pm 2.5$ and $p_T(\gamma) > 100$ GeV. Cuts are also made on $\Delta R_{\ell\gamma} > 0.7$ and on the invariant mass of the charged lepton pair, $M_{\ell\ell} > 10$ GeV.

It is clear from Figs. 6 and 7 that the anomalous couplings h_i^V can produce an increase in cross section for the $p_T(\gamma)$ approximately an order of magnitude larger than the SM, if taken at their current limits. The response is the same for both $ZZ\gamma$ and $Z\gamma\gamma$ production. The couplings h_1^V and h_3^V fall off slightly faster than h_2^V and h_4^V . The tightest limits will be set by a careful study of this distribution.

In the $q\bar{q} \rightarrow Z\gamma$ subprocess the effects of anomalous $ZZ\gamma$ and $Z\gamma\gamma$ couplings are enhanced at large energies. If the Z boson decays into a pair of charged leptons, a typical signal for anomalous couplings will be a broad increase in the Z-photon invariant mass spectrum at large values of $M_{Z\gamma} = \sqrt{s}$, possibly cutting off above $M_{Z\gamma} = \Lambda$, the form factor scale [28]. Because of the finite detector resolution effects, the Z-boson resonance is broadened, and the peak cross-section is significantly reduced.

Fig. 8 shows the $d\sigma/dM_T(\ell\ell\gamma)$ spectrum for different CP-violating anomalous coupling constants: the SM ($h_i^V=0$), the tightest current limit on $h_1^V (=0.5$ with $h_2^V=0$), and the tightest current limit on $h_2^V (=0.05$ with $h_1^V=0$). Fig. 9 shows the $d\sigma/dM_T(\ell\ell\gamma)$ spectrum for different CP-conserving anomalous coupling constants: the SM ($h_i^V=0$), the tightest current limit on $h_3^V (=0.5$ with $h_4^V=0$), and the tightest current limit on $h_4^V (=0.05$ with $h_3^V=0$). A form factor scale of $\Lambda=750$ GeV was used. The variation in the distribution due to the anomalous couplings is clearly visible. The cuts used in Figs. 8 and 9 were $\eta < \pm 2.5$ and $p_T(\gamma) > 100$ GeV, $p_T(\ell) > 10$ GeV, $\Delta R_{\ell\gamma} > 0.7$ and $M_{\ell\ell} > 10$ GeV.

It is clear from Figs. 8 and 9 that the anomalous couplings h_i^V produce an increase in cross section for the $M_T(\ell\ell\gamma)$ approximately an order of magnitude larger than the SM. The response is the same for both $ZZ\gamma$ and $Z\gamma\gamma$ production. The couplings h_1^V and h_3^V fall off slightly faster than h_2^V and h_4^V .

For the purpose of this study only the $p_T(\gamma)$ and $M_T(\ell\ell\gamma)$ spectra have been investigated. Both distributions clearly show the presence of anomalous couplings when compared to the expected SM distributions. They will therefore be useful tools in the study of anomalous couplings at the LHC.

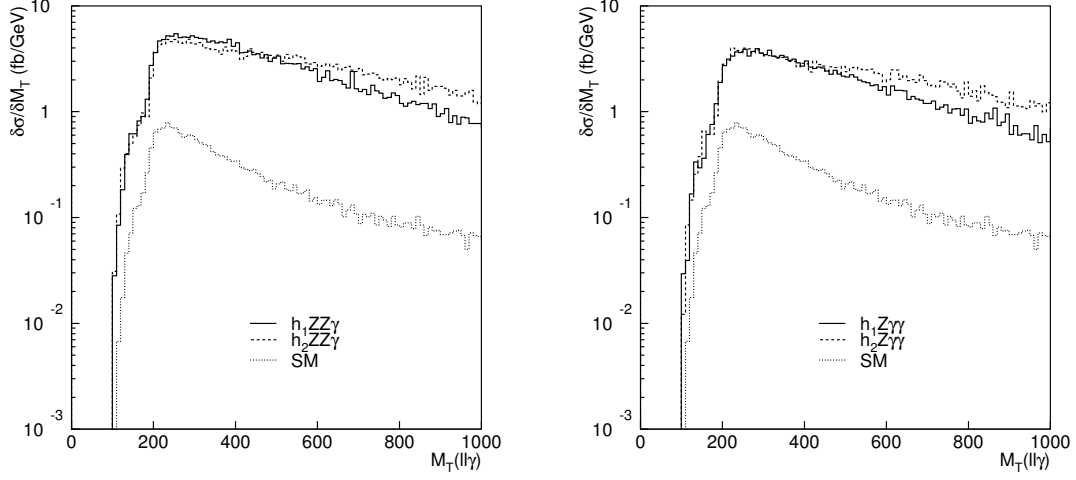


Figure 8: $d\sigma/dM_T(\ell\ell\gamma)$ spectrum for the SM ($h_i^V=0$) and anomalous CP-violating coupling limits ($h_1^V=0.5$ and $h_2^V=0.05$) at $\Lambda = 750$ GeV for (left) the $ZZ\gamma$ vertex and (right) the $Z\gamma\gamma$ vertex

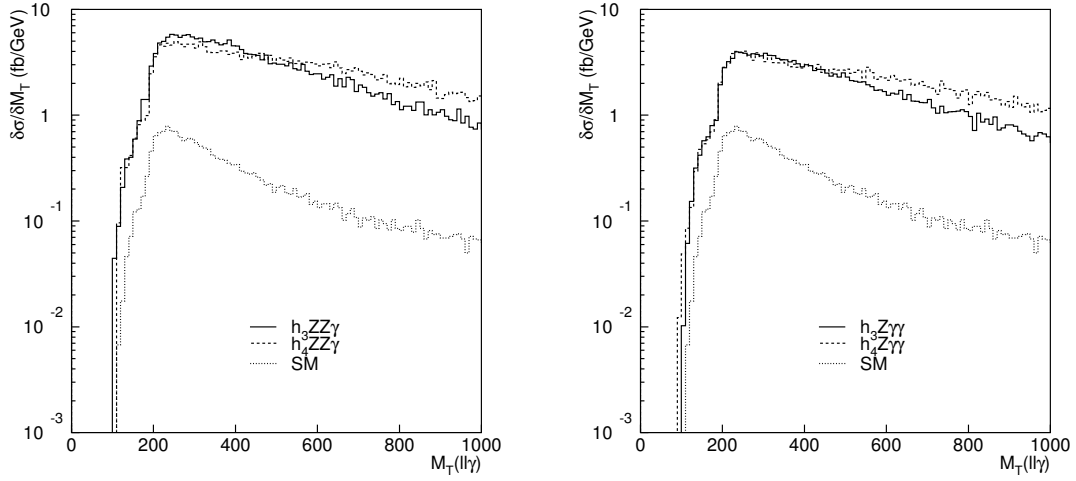


Figure 9: $d\sigma/dM_T(\ell\ell\gamma)$ spectrum for the SM ($h_i^V=0$) and anomalous CP-conserving coupling limits ($h_3^V=0.5$ and $h_4^V=0.05$) at $\Lambda = 750$ GeV for (left) the $ZZ\gamma$ vertex and (right) the $Z\gamma\gamma$ vertex

The $Z\gamma$ events in a pp collider are produced by a collision of a valence quark and a sea anti-quark, with the production of an off-shell Z . This radiates a photon to become on-shell. Fig. 10 (a) shows a schematic of the production in the lab. frame and (b) shows a schematic of the production in the centre of mass frame of the Z .

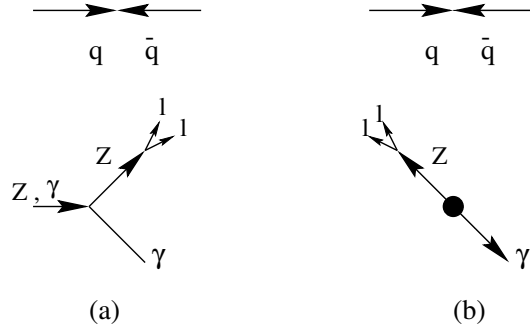


Figure 10: Schematic of the signal production in the lab. frame and (b) in the centre of mass frame

On average the quarks in a proton have a harder momentum distribution than the anti-quarks, which originate from the sea. As a result the Z^* is likely to be produced in the direction of the quark rather than the anti-quark and the energy of the Z^* will be much greater than its momentum.

If the fundamental process is as shown in fig. 10 (a), then the events may divide into two classes, $Z^* \rightarrow$ and $\leftarrow Z^*$. In both cases $p_T(\gamma) = p_T(Z)$. The helicity of the leptons tends to follow that of the initial Z^0 . Therefore a correlation between ϕ_γ and ϕ_ℓ would be expected. Fig. 11 shows the ϕ correlation between the lepton and isolated photon from the $Z\gamma$ event. The ϕ distributions show clearly the expected correlation with an excess of events at π .

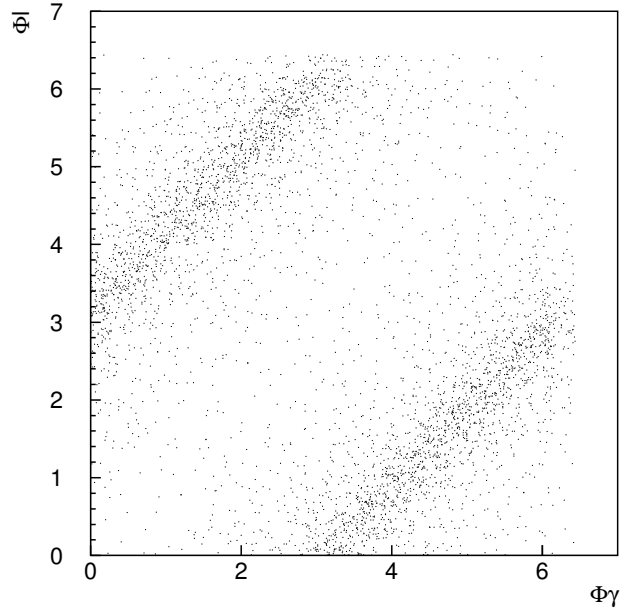


Figure 11: ϕ correlation of the lepton and photon

Fig. 12 shows the θ correlation between the lepton and isolated photon. The θ distributions are clearly anti-correlated. Fig. 13 shows the η correlation between the lepton and isolated photon. The η distributions are clearly correlated, peaking at $\eta=0$. For the case of massless particles η is exactly equal to the rapidity of the system, y .

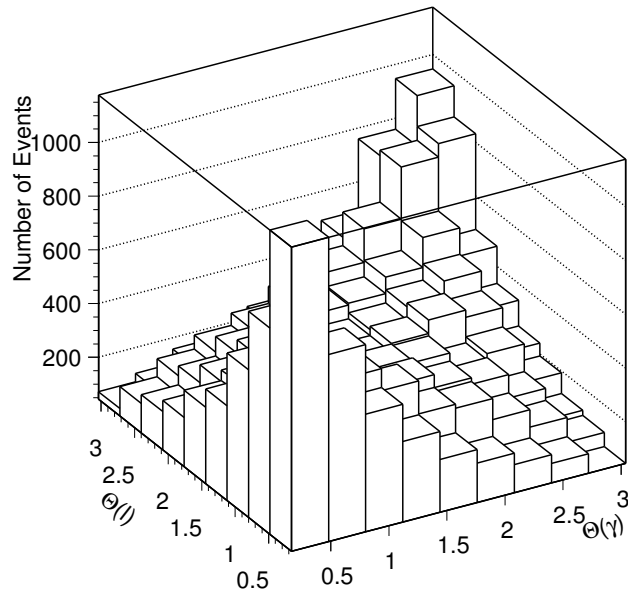


Figure 12: Θ correlation of the lepton and photon

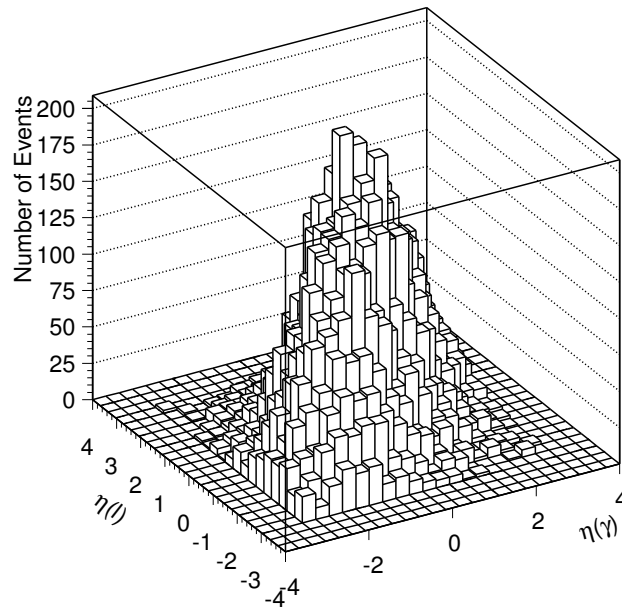


Figure 13: η correlation of the lepton and photon

By combining the BAUR generator with the CMSJET 4.3 detector simulation and making use of Pythia, $Z\gamma$ events with anomalous couplings can be generated and the response of the detector evaluated. This enables the study of the SM $Z\gamma$ signal and of the sensitivity of CMS to the anomalous couplings.

The anomalous couplings are easily identifiable when examining the $p_T(\gamma)$ distribution by an increase in cross section at high p_T . It will also be possible to use the $M(\gamma\ell\ell)$ distributions to study the anomalous couplings. There is an increase in the cross section at high $M(\gamma\ell\ell)$ for the anomalous couplings. This is true for both the $ZZ\gamma$ and $Z\gamma\gamma$ vertices and for both the CP-conserving and CP-violating couplings.

5 Conclusion

This study shows that CMS will be able to observe anomalies in the $ZZ\gamma$ and $Z\gamma\gamma$ vertices using both the $p_T(\gamma)$ spectrum and the $M_T(\ell\ell\gamma)$ distribution. There is a notable increase in the cross sections of both spectra when the anomalous couplings vary from the SM value of zero. Performing a likelihood fit to either spectra would enable the sensitivities of h_1^V , h_2^V , h_3^V and h_4^V ($V=Z,\gamma$) to be evaluated.

The BAUR generator has been successfully integrated with CMSJET to provide a combined generator and detector simulation which includes the NLO QCD corrections which are very important at the LHC. Using this simulation the $Z\gamma$ signal has been studied for both SM and anomalous couplings. Further work is being completed on the backgrounds to these signals and hence values for the sensitivity of CMS to these anomalous couplings will be made.

Acknowledgements

We would like to thank Prof. U. Baur of SUNY Buffalo for providing the generator and for many helpful discussions.

References

- [1] C. K. Mackay, P. R. Hobson, “*Observing anomalous di-boson couplings in the $WW\gamma$ vertex at CMS*” CMS Note 052 (2001)
- [2] C. K. Mackay, P. R. Hobson “*Sensitivity of CMS to CP conserving anomalous di-boson couplings in $W\gamma$ events*” CMS Note 056 (2001)
- [3] H. Aihara et al., “*Anomalous gauge boson interactions*” Electroweak symmetry breaking and new physics at the TeV scale, World Scientific, eds. T. Barklow et al., p488
- [4] S. Godfrey, “*Quartic gauge boson couplings*” International Symposium on Vector Boson Interactions, Edited by U. Baur, S. Errede and T. Muller. AIP Press (1996) p261
- [5] E. Leader, E. Predazzi, “*An introduction to gauge theories and modern particle physics*” Electroweak Interactions, the “new physics” and the parton model, Volume 1, Cambridge Monographs on Particle Physics, Nuclear Physics and Cosmology, Cambridge University Press, Cambridge U.K. (1996) p55
- [6] D. Fouchez, “*Gauge boson pairs production study with Atlas*” ATLAS IN 060 (1995)
- [7] H. Kuijf et al., “*Parton luminosities, W and Z cross sections and gauge boson pair production*” Large Hadron Collider Workshop, Aachen, CERN 90-10, ECFA 90-133 (1990) p91
- [8] E. Maina, S. Moretti, “ *Z^0, γ production in association with top quarks*” Phys. Lett. B286 370 (1992)
- [9] E. Nuss, “*Di-boson production at hadron colliders with general triple gauge boson couplings*” Z. Phys. C76 701 (1997)
- [10] C. K. Mackay, “*The electromagnetic calorimeter for CMS and a study of the $WW\gamma$ vertex*” CMS Ph.D. Thesis, Brunel University, Uxbridge, UK (1998) CMS/1999-012 THESIS, RAL-TH-1999-001, ISSN 1362-0215

- [11] M. Reichel, “*Simulationsstudien zur $W\gamma$ produktion in hadronischen kollisionen bei CDF und CMS*” Karlsruhe Internal Report IKEP-KA-98-06 (1998) Unpublished
- Th. Muller, D. Neuberger, W. H. Thummel, “*Sensitivities for anomalous $WW\gamma$ and $ZZ\gamma$ couplings at CMS*” CMS Note 017 (2000)
- [12] S. Weinberg, “*Phenomenological Lagrangians*” Physica 96A 327 (1979)
- [13] G. Gounaris & F. Renard, “*The anomalous 3-boson couplings as an implication of the Higgs sector*” Z. Phys. C59 133 (1993)
- [14] T. Rizzo, “*Looking for weak-boson compositeness via form factors*” Phys. Rev. D32 43 (1985)
- [15] K. Hagiwara, R. Peccei, D. Zeppenfeld, K. Hikasa, “*Probing the weak boson sector in $e^+e^- \rightarrow W^+W^-$* ” Nucl. Phys. B282 253 (1987)
- [16] U. Baur, E. Berger, “*Probing the weak-boson sector in $Z\gamma$ production at hadron colliders*” Phys. Rev. D47 4889 (1993)
- [17] U. Baur, T. Han, J. Ohnemus, “*QCD corrections and anomalous couplings in $Z\gamma$ production at hadron colliders*” Phys. Rev. D57 2823 (1998)
- [18] Particle Data Group, K. Hikasa et al., “*Review of particle physics*” Phys. Rev. D45 S1 (1992)
- [19] The LEP Collaborations and the LEP GC Working Group., “*Combined Preliminary Results on Electroweak Gauge Boson Couplings Measured by the LEP Experiments*” LEPEWWG/TGC/2001-01 (2001)
- [20] D0 Collaboration, “*Measurements of Trilinear Gauge Boson Couplings*” ICHEP 98 Conference, Vancouver, (1998) to be published
- [21] D. Amidei, R. Brock, “*Future electroweak physics at the FERMILAB tevatron*” Report of the TeV2000 study group, FERMILAB-PUB-96-082 (1996)
- [22] T. Sjostrand, “*PYTHIA 5.721 and JETSET 7.408 generators*” Comp. Phys. Comm. 82 74 (1994)
- [23] J. Ohnemus, “*Order- α_s calculations of hadronic $W^\pm\gamma$ and $Z\gamma$ production*” Phys. Rev. D47 940 (1993)
- [24] J. Ohnemus, “*QCD corrections to diboson production*” International Symposium on Vector Boson Interactions, Edited by U. Baur, S. Errede and T. Muller. AIP Press (1996)
- [25] J. F. Owens, “*An updated set of parton distribution parametrizations*” Phys. Lett. B266 126 (1991)
- [26] V. Barger et al., “*Pair production of W^\pm, γ and Z in association with jets*” Phys. Rev. D41 2782 (1990)
- [27] The Particle Data Group, “*Review of particle physics*” European Physics Journal C Vol. 15 1-4 (2000)
- [28] U. Baur, D. Zeppenfeld, “*Probing the $WW\gamma$ vertex at the future hadron colliders*” Nucl. Phys. B308 127 (1988)
- [29] U. Baur, T. Han, J. Ohnemus “*QCD corrections to hadronic $W\gamma$ production with non standard $WW\gamma$ couplings*” Phys. Rev. D48 5140 (1993)
- [30] S. Abdullin, A. Khanov, N. Stepanov, “*CMSJET 4.3*” CMS NOTE 180 (1994)
- [31] B. Flaugher, K. Meier, “*A compilation of jet finding algorithms*” Proc. of the Summer Study on Physics, Snowmass (1990)

The BAUR generator builds up the $Z\gamma$ events from 3 processes: $2\rightarrow 4$ body decay, $2\rightarrow 3$ body decay and photon bremsstrahlung. The NLO cross section for hadronic $Z\gamma$ production [23] consists of two- and three- body final state contributions:

$$\sigma^{NLO}(pp \rightarrow Z\gamma + X) = \sigma_{2\text{-body}}^{NLO}(pp \rightarrow Z\gamma) + \sigma_{3\text{-body}}(pp \rightarrow Z\gamma + X) \quad (7)$$

where the two body contribution is ²⁾:

$$\sigma_{2\text{-body}}^{NLO}(pp \rightarrow Z\gamma) = \sigma_{Brems}^{NLO} + \sigma^{HC} + \text{combined terms}$$

where the quantities σ_{Brems}^{NLO} and σ^{HC} are the contributions from the NLO bremsstrahlung cross section and the hard collinear remnants respectively.

In order to calculate the NLO corrections the soft and collinear singularities associated with the real emission subprocesses must be isolated [23] [29]. This is done by partitioning phase space into soft, collinear and finite regions, and introducing theoretical soft and collinear cutoff parameters δ_s and δ_c . The individual contributions to the cross section are dependent on the collinear and soft cutoff parameters. The 3- and 4-body contributions, which separately have no physical meaning, vary strongly with δ_s and δ_c [29]. However, the total cross section, which is the sum of the 3- and 4-body and bremsstrahlung contributions, is independent of δ_s and δ_c over a wide range of these parameters.

If δ_s and δ_c are too small, then the 3-body contributions to the total cross section can have a negative weighting, although the overall value remains unchanged. In order to assure positive weightings for the 3-body contribution the optimum values for δ_s and δ_c must be evaluated for the LHC conditions. Generating 10,000 events with standard model values for h_i^V the cross section was calculated with one parameter varying at a time.

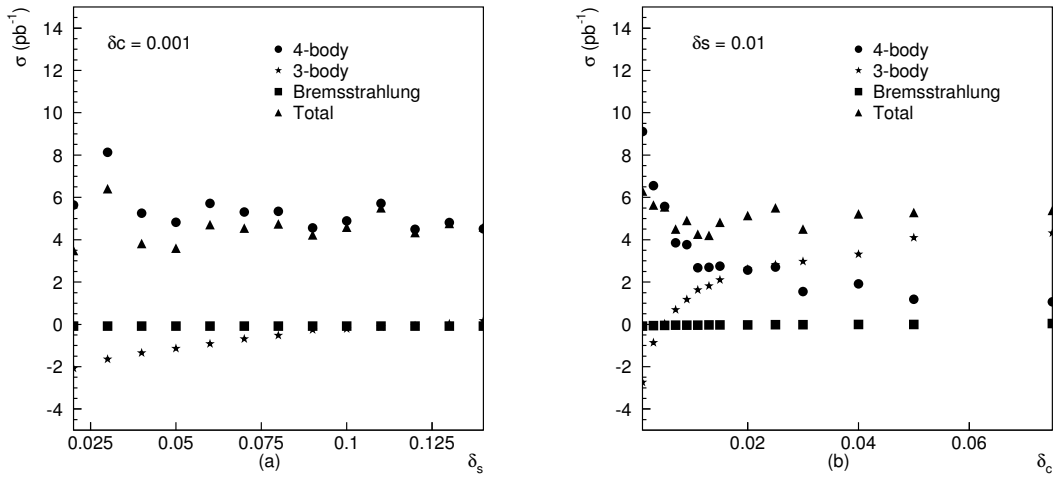


Figure 14: The individual contributions to (a) the soft cutoff parameter and (b) the collinear cutoff parameter

Fig. 14 (a) and (b) show the variation of the cross section with each parameter for the 4-body, 3-body, bremsstrahlung and total contributions. The optimum values chosen were $\delta_s = 0.08$ and $\delta_c = 0.05$.

²⁾ See the appendices of [29] for a full derivation of the contributions.

CMSJET [30] is a stand-alone fast non-GEANT detector simulation of the CMS detector which is essentially generator independent. CMSJET passes the first event through a selection of kinematic cuts and then proceeds to the next event. Assuming the event passes these cuts, user defined cuts are then applied to the particles in the event table allowing, for example, a minimum p_T for leptons and photons. This allows particles which would not be selected by the CMS trigger to be rejected. A calculation of the missing energy is also made.

The remaining particles are then passed through the various sub-detectors. Particles such as photons and electrons will interact in the electromagnetic calorimeter. The energy deposited in the calorimeter is calculated using a parameterisation of the sub-detector. Similar methods are used for particles in the hadron and very forward calorimeters. The muon chambers are dealt with in a simpler way. The momenta is smeared and only those muons able to produce a hit in the muon system are taken into account.

The final analysis phase includes jet-finding, calculating the measured the missing energy and applying quark tagging efficiencies. Following this the relevant data are written out for subsequent analysis.

The CMSJET calorimeter system is represented by a set of sectioned cylindrical volumes. Charged particles are traced through the uniform 4 tesla magnetic field up to the surface of the calorimeter system. The energy/momentum of the particles are smeared according to the resolutions shown in Table 3. The showers' spatial development is then simulated in both lateral and longitudinal directions. The parameterisations for the showers is taken from the H1 experiment. It should be noted that hadronic showers are also allowed to start in the electromagnetic calorimeter.

Table 3: Calorimetry in CMSJET 4.3

Sub-detector	Resolution
ECAL	$\sigma/E = 5\%/\sqrt{E} + 0.5\%$
HCAL	$\sigma/E = 82\%/\sqrt{E} + 6.5\%$
HCAL crack	$\sigma/E = 86\%/\sqrt{E} + 9.3\%$
VFCAL (hadrons)	$\sigma/E = 182\%/\sqrt{E} + 9.0\%$
VFCAL (e, γ)	$\sigma/E = 138\%/\sqrt{E} + 5.0\%$

Jets are searched for in the ECAL and HCAL out to a rapidity $|\eta|=3.0$ with the UA2 jet finding algorithm [31]. Using the full granularity of both ECAL and HCAL an initial selection is performed that rejects any calorimeter deposit (cell) with $E_t < 1\text{GeV}$. A pre-clustering stage then takes each cell in turn and adds to it any nearby cells which pass the criterion

$$\Delta R = \sqrt{(\Delta\phi^2 + \Delta\eta^2)} \text{ where } \Delta R < 0.3$$

with no restriction on the number of pre-clusters a given cell may belong to. Overlapping pre-clusters that share 75% or more of their cells are joined together otherwise they are split apart with the cells going to the closest initiator cell. The remaining pre-clusters that have total $E_t > 20\text{ GeV}$ are designated jets. Finally, any cell that fails the initial selection stage or the 20 GeV cut are added to the nearest jet providing that $\Delta R < 0.3$. Once identified, each jet is labelled or tagged to the type of quark or gluon that initiated the jet.

Since high p_T π^0 s can often be misidentified as a photon, they may form an irreducible background to the $Z\gamma$ signal, and must therefore be well studied. Using CMSJET 4.3 it is possible to prevent the π^0 decay straight away and to study their characteristics before forcing their decay and then seeing how many of the photons from the π^0 decays are misidentified as isolated photons.

CMSJET 4.3 was used for all the work in this study, although there now exist later versions which include the final detector designs. The most obvious inaccuracy for the case of this study was in the CMS ECAL endcap and plug designs. The resolutions for the ECAL were poorer than the latest test beam results, providing a slightly pessimistic scenario.